

Low Frequency Quantum Transport in a Three-probe Mesoscopic Conductor

Qingrong Zheng and Jian Wang

Department of Physics,
The University of Hong Kong,
Pokfulam Road, Hong Kong.

Hong Guo

Centre for the Physics of Materials,
Department of Physics, McGill University,
Montreal, Quebec, Canada H3A 2T8.

The low frequency quantum transport properties of a three-probe mesoscopic conductor are studied using Buttiker's AC transport formalism. The static transmission coefficients and emittance matrix of the system were computed by explicitly evaluating the various partial density of states (PDOS). We have investigated the finite size effect of the scattering volume on the global PDOS. By increasing the scattering volume we observed a gradual improvement in the agreement of the total DOS as computed externally or locally. Our numerical data permits a particular fitting form of the finite size effect.

PACS number: 72.10.Bg, 73.20.Dx, 73.40.Gk, 73.40.Lq

1 Introduction

In recent years extensive investigations of ballistic and mesoscopic quantum conductors have been carried out [1]. Experimentally the advances in nanotechnology have enabled the possibility of fabricating submicron structures with linear size of 1000 Angstrom or less. Due to quantum size effect, the transport properties of these small systems can be very different from their classical counterpart and many interesting phenomena have been discovered [1]. On the theoretical side, a main tool for understanding static ballistic transport is based on the scattering approach of Landauer-Buttiker formalism [2, 3].

It has been realized that the usual static scattering approach can not be directly applied to dynamic transport problems where the external potential has a time dependent oscillating component. As shown by Buttiker and his co-workers, a direct application of the original approach of Landauer-Buttiker formalism can not yield electric current and charge conservation. To preserve this conservation, it is necessary to consider the implication of the long range Coulomb interaction. As a result the AC transport theory for coherent quantum conductors are more complicated. At present there are several approaches to deal with the problem of computing AC conductance. In a strongly correlated electronic system, the Anderson impurity model is often used. To treat AC transport one employs the linear response theory in conjunction with the Keldysh Green's function which is often applied to deal with non-equilibrium problems [4]. One can also use Kubo's linear response theory by assuming that the electric field inside the sample is known a priori. However this is a very strong requirement [5].

Along another line of development Buttiker and his co-workers have advanced a current conserving formalism [6]. The key idea in this theory is to consider the self-consistent internal potential so that the current and the charge is conserved. In a series of articles, Buttiker and co-workers investigated several low frequency quantum transport problems [6, 7, 8, 9, 10, 11]. To first order in frequency ω , the response of an arbitrary scattering problem to quasi-static perturbations in the scattering potential is naturally expressed in terms of a set of local partial density of states (PDOS) each associated with one element of the scattering matrix. This AC transport formalism has also been extended to second order in frequency ω in the quantum hall regime [11].

The application of Buttiker's AC transport theory is easier in 1D, such as a 1D quantum well, a δ -function potential, and a perfect quantum wire, where the scattering matrix and wave function can be obtained analytically. Much

intuition and interesting results have been obtained from 1D calculations which can often be done analytically. The investigations for 2D conductors have recently begun [12, 13, 14, 15] and the dynamic transport response of a 3D atomic wire has been calculated using first principles [16]. However, due to technical difficulties, in 2D one usually can not obtain analytical expressions for the AC admittance except for very special cases [13, 14]. For more general situations numerical calculations are needed.

It is the purpose of this article to further investigate AC admittance of 2D coherent conductors in the ballistic regime. In particular we shall focus on numerically analyzing a three probe conductor as shown in Figure (1). There are several motivations for this study. First, similar to that of the DC transport situation [1], we believe coherent AC admittance of multi-probe (by multi-probe we mean more than two probes) conductors should be studied in detail since usually experimental measurements are conducted in multi-probe setups. However to the best of our knowledge there is as yet a detailed numerical analysis of any 2D multi-probe systems. Second, in our investigations of two-probe conductors [12, 13], an important technical point is the size effect of the scattering volume. It was found [18, 12, 13] that the total PDOS as computed from external global PDOS (GPDOS) does not equal to that computed from the local PDOS (LPDOS), unless the scattering volume is very large. This led to a violation of the current conservation and gauge invariance in numerical calculations where the scattering volume is always finite. Hence there is a need to explicitly and systematically examine the scattering volume size effect. Finally, in order to study certain physical effects such as the inelastic and dissipative effects using the quantum scattering approach, a very useful phenomenological approach is to introduce fictitious links from the conductor to external dissipative reservoirs [17]. In this case one must deal with multi-probe situations.

To these purposes we have computed the low frequency admittance of a three-probe junction (see Fig. (1)). We have examined the emittance matrix for both the tunneling regime and the transmissive regime in detail. The behavior of the emittance matrix is found to be closely related to that of the transmission coefficients. We have computed the total PDOS from both the external GPDOS and the local LPDOS, and largely speaking the two total PDOS as obtained approach each other as the scattering volume is increased. We found that there exists a "critical region" in energy near the second propagating subband threshold, such that within this region the charge conservation is not strictly obeyed for any finite scattering volume. However the larger the scattering volume, the smaller the

"critical region" is.

This paper is organized as the following. In the next section we set out the theoretical and numerical procedures of computing the transmission functions. In section III we present and analyze the numerical results. Both the dynamic and static transport properties and their relationship will be discussed. Finally, a summary is given in section IV.

2 Theoretical and numerical analysis

The current conserving dynamic transport formalism proposed by Buttiker and co-workers is amply reviewed in several articles [19] and we refer interested readers to them. In this section we shall only outline our theoretical and numerical procedures to compute the necessary quantities such as the various partial density of states for the 3-probe system.

It has been shown by Buttiker, Thomas, Prêtre, Gasparian and Christen [3, 6, 7, 18], to linear order in frequency ω the admittance is given by the following formula,

$$g^I(\omega) = g^e(\omega = 0) - i\omega e^2 E \quad (1)$$

where the emittance matrix E is calculated from the various partial density of states:

$$E = \frac{dN}{dE} D : \quad (2)$$

The subscripts $\alpha\beta$ indicates scattering from a lead labeled by α to that labeled by β . The first term in the emittance matrix gives the AC response of the system to the external potential change, while the second term is from the internal potential change induced by the external perturbations. The external contribution is determined by the global partial density of states [9]: for a large scattering volume the global PDOS can be expressed in terms of the energy derivative of the scattering matrix elements [20]

$$\frac{dN}{dE} = \frac{1}{4} \sum_{\alpha\beta} S_{\alpha\beta}^y \frac{ds}{dE} = \frac{ds^y}{dE} S_A : \quad (3)$$

On the other hand the internal contribution D is related to the local PDOS, and within the Thomas-Fermi linear screening model is given by

$$D = \sum_{\alpha\beta} \int dr \frac{dn(\mathbf{r}; \omega)}{dE} \frac{dn(\mathbf{r})}{dE} = \sum_{\alpha\beta} \int dr \frac{dn(\mathbf{r}; \omega)}{dE} ; \quad (4)$$

where the local PDOS (called injectivity) is calculable from the scattering wavefunction,

$$\frac{dn(r; \epsilon)}{dE} = \frac{1}{hJ} j(r)^2 : \quad (5)$$

where J is the incident flux and $j(r)$ is the scattering wavefunction for electrons coming from the probe ϵ . In the absence of a magnetic field, the emissivity $dn(\epsilon; r)/dE$ equals to the injectivity [11]. Finally, $dn(r)/dE = \sum_P dn(\epsilon; r)/dE$ is the total local density of states. It is straightforward to prove that the current is conserved since the admittance matrix g^I satisfies $\sum_P g^I(\epsilon) = 0$. This can be seen by realizing that $\sum_P dN/dE = dN/dE$ is the injectance which is identical to $\sum_P D$.

To compute the various PDOS, for simplicity we shall focus on the first transport subband only, thus the incoming electron energy is restricted to within the interval $(-\hbar a)^2 < E < (2\hbar a)^2$ in units of $\hbar^2 = (2ma^2)$ with m the effective mass of the electron and a the width of the leads (see Fig. (1)). Multi-subbands can also be included without difficulties, such as that of Ref. [16]. The scattering properties of the three-probe system is then characterized by a 3×3 scattering matrix $S(E)$ satisfying $S_{\alpha\beta} = 1; 2; 3$. For example, for an incident electron coming from probe 1, it scatters in the scattering volume, and then reflects back to probe 1 with a probability amplitude given by S_{11} , or transmits to probes 2 and 3 with probability amplitudes S_{21} and S_{31} , respectively. The transmission coefficients can thus be expressed in terms of scattering matrix, i.e. $T_{\alpha\beta} = S_{\beta\alpha}^*$. For the system of figure (1), the scattering matrix has the following symmetry: $S_{11} = S_{22}$; $S_{21} = S_{12}$; $S_{31} = S_{32}$; $S_{13} = S_{23}$ and $S_{13} = S_{31}$. Therefore, there are only four distinct elements out of nine.

For the three-probe conductor of Figure (1), the quantum scattering problem is solved using a mode matching method. The wavefunction in region I can be written as

$$\psi_I = \sum_n \psi_n(y) (a_n e^{ik_n x} + b_n e^{-ik_n x}); \quad (6)$$

where $\psi_n(y)$ is the transverse wave function, $k_n^2 = E - (\hbar a)^2$ is the transport energy, a_n is the input parameter, and b_n is the reflection amplitude. Similarly for region II, we have

$$\psi_{II} = \sum_n \psi_n(y) (c_n e^{ik_n x} + d_n e^{-ik_n x}) : \quad (7)$$

For region III,

$$\psi_{III} = \sum_n \psi_n(x) (e_n e^{ik_n y} + f_n e^{-ik_n y}); \quad (8)$$

where c_n and e_n are transmission amplitudes and d_n and f_n are input parameters. The wavefunction in region IV is the combination of wavefunctions in regions I, II, and III. At the boundaries of the various regions, we match the wavefunctions and their derivatives and this leads to the desired transmission coefficients with which the scattering wave functions Eqs. (6)–(8) are also determined.

If we choose point O as the origin (see figure 1), the scattering matrix s_1 is defined as

$$\begin{aligned} s_{11} &= b_1 \\ s_{12} &= c_1 e^{ik_1 a} \\ s_{13} &= e_1 e^{ik_1 a} : \end{aligned} \quad (9)$$

Using Eqs. (2)–(5) and the solution of the scattering problem, we can explicitly compute the low frequency admittance.

3 Results

We have investigated the transmission coefficient and the admittance matrix in two different transport regimes for various system parameters. The first regime is very transmissive and the second is a tunneling regime where tunnel barriers are added at the probes. The AC response of these regimes can be quite different as a transmissive situation tends to be inductive, while a non-transmissive case tends to be capacitive (see below). The low frequency admittance is given by Eq. (1) in which the DC conductance g^e ($\neq 0$) of our three-probe system is determined using transmission coefficients by applying the Buttiker multi-probe conductance formula [3].

3.1 Admittance

In Figure (2) we show the transmission coefficients and the admittance E in the transmissive regime as a function of the incoming electron energy. In this case the system does not show any resonance behavior and the transmission coefficients T (E) are quite large for most of the energy range while the reflection coefficient R_{11} is small (Fig. (2a)). It is interesting to find that the shape of admittance are similar to that of the corresponding transmission coefficients, as shown in Fig. (2b). This is different from cases where quantum resonances dominate the transport [12] (see below) and for that case the AC responses follow the DC transmissions only at the resonances.

There are two different responses to the external time varying potential: capacitive and inductive depending on the sign of the emittance matrix element E_{11} . According to Eq.(2), E_{11} consists of two terms: $dN_{11}=dE$ the capacitive term and D_{11} the inductive term. For a two probe capacitor there is no DC current so that $dN_{12}=dE = 0$. As a result E_{12} is negative. Therefore for a capacitor $E_{11} = -E_{12}$ is positive. Extending this notion, one concludes that the system responds capacitively if E_{11} is positive. For a ballistic conductor with complete transmission $dN_{11}=dE$ vanishes and E_{11} is negative. In other words, negative E_{11} gives an inductive response. These different responses are clearly shown in Fig. (2).

The AC transport properties are very different in the tunneling regime. To establish such a regime, we have put tunneling barriers inside probes 1 and 2 at the junctions between the probes and the scattering volume. In particular the barrier heights are $V_{\text{barrier}} = 40E_1$, and the width is 0.1 where the width of the wire has been set to one. No barrier is added in probe 3. We have also included a potential well with depth $V_{\text{well}} = -40E_1$ in the center of the scattering volume with a size of 2.8 : 1.9. The well and barriers establish several transport resonances, these are clearly marked by the sharp peaks in the electron dwell time defined as [21]

$$\tau = \frac{1}{J} \int_{\text{sc}} \langle \hat{n}(\mathbf{r}) \rangle d^3r ; \quad (10)$$

where τ is the scattering volume. τ is plotted against energy in Fig. (3) while the inset shows τ_3 . The dwell time measures the duration an electron spends in the scattering volume. Thus if transport is mediated by resonance states we expect much longer dwell times [22] at the resonances. This idea has recently been proved by Iannacone [23]. Fig. (3) shows that three resonance states, with energies $E_1 = 13.2$, $E_2 = 24.1$ and $E_3 = 35.6$ are established. The quantum resonances also leads to sharp peaks in the transmission coefficient T_{21} and reflection coefficient R_{11} , as shown by the solid lines of Fig. (4a,4b). At these resonances both the GPDOS and LPDOS take maximum values, leading to the sharp jumps in the emittance E_{11} and E_{21} as shown by the data points in Fig. (4a,4b). The variations of E_{11} and E_{21} as functions of energy E are very closely correlated with those of $R_{11}(E)$ and $T_{21}(E)$ near the resonances, as shown by Fig. (4). Since there was no tunneling barrier in probe 3, the resonance transmission to that probe is not as sharp, and the transport behavior shows a mixture of tunneling and transmissive nature, as shown in Fig. (4c).

In the tunneling regime the AC response changes sharply from inductive at

one side of the resonance energy to capacitive on the other side of the resonance or vice versa, in distinctive difference as compared to the transmissive case discussed above. Let's examine E_{11} near resonance E_3 . As the energy approaches to E_3 , the system first responds inductively and is followed by a strong capacitive response. This behavior is clearly related to the fact that the resonance is characterized by a complete reflection indicated by the large peak in the reflection coefficient (see Fig. (4a)). This behavior has been seen previously in 2D quantum wires[13]. On the other hand, for 1D resonance tunneling, a Breit-Wigner type transmission resonance gives rise to the similar AC response behavior[7] discussed here. When the incident energy is near the resonance E_1 , the AC response is reversed: first capacitively and then inductively. Hence the behavior near E_1 and E_3 are very different. For energy near E_1 the emittance behaves like an odd function but near E_3 it is like an even function. The reason, as we have checked numerically, is that the external and the internal responses do (not) reach the maximum at the same energy for E near E_3 (E_1). This behavior of E_{11} is also a manifestation of the reflection coefficient R_{11} . As energy sweeps through E_1 , the strong capacitive AC response is due to the complete reflection peak, and the following inductive response is because the reflection coefficient $R_{11} = 0$. Hence in the AC response of a system, near a quantum resonance whether it is voltage following current (capacitive) first, or current following voltage (inductive) first, can only be determined by detailed analysis and the outcome depends on the peculiarities of the system such as the existence of a third probe as we have studied here. In Figure (4c) we show the emittance matrix elements E_{13} . Although they have much smaller values they do exhibit dips around three resonant energies E_1 , E_2 , and E_3 .

3.2 Finite size effect of the GPDOS

A very important formal advance of the AC transport theory is the correct characterization of electric current conservation. In principle this requirement is satisfied by the AC transport formalism used here[6] which demands $\sum_P E = 0$. Hence we must have $\sum_P dN = dE = \sum_P D$. Since both sides of this equation represent the total scattering DOS, thus the current conservation is obtained. In practical calculations, the left hand side of this equation is computed externally, using the scattering matrix which is calculated at the boundaries of the scattering volume. On the other hand the right side of this equation is calculated locally, using the scattering wavefunction inside the scattering volume. These two quan-

tities become precisely equal when the scattering volume is very large [19]. For a finite scattering volume, correction terms should be added to the GPDOS, as shown in Ref. [24] for 1D systems, and in Ref. [13] for a 2D system. Without the corrections, numerical results for a 2D quantum wire showed a small but systematic deviation from the precise current conservation [12]. Such a deviation actually diverges at the edges of successive propagation subbands as shown in Ref. [13].

Since partial density of states play a vital role in the AC transport formalism used in this work, in this section we present a detailed analysis of the finite size effect of the scattering volume to the GPDOS. To this purpose we have examined a variety of system sizes L for many energies near the onset of the second transport subband. As a measure, we define a quantity which is the difference of the total DOS as calculated from GPDOS and LPDOS:

$$\Delta N = \int_{E_1}^{E_2} \frac{dN}{dE} dE \quad (11)$$

Obviously $\Delta N = 0$ if the current is precisely conserved.

Fig. (5a) shows ΔN as a function of the system size L for three energies very close to the second subband edge which is located at $E_2 = 39.4784$. A clear crossover to the large volume limit is revealed as $\Delta N \rightarrow 0$ when L is increased. It is also clear that for energy closer to E_2 , the crossover is slower (solid line). We found that the decay of ΔN is essentially exponential for all energies examined, and has an interesting form for large L :

$$\Delta N \sim e^{-k_2(2L+1)} \quad (12)$$

where $(2L+1)$ is precisely the scattering volume length from probe I to probe II, and k_2 is the momentum corresponding to the second subband energy E_2 . We have plotted $-\ln[\Delta N/(2L+1)] = k_2$ in Fig. (5b) for several energies. Our numerical data supports Eq. (12) quite well for large L , and for energies closer to E_2 . It is not difficult to understand the form of Eq. (12). Due to the scattering at the junction where the three probes meet, complicated mode mixing takes place. While the incoming electron is in the first subband, mode mixing generates wavefunctions for many higher subbands, including the second subband, which become evanescent in the probes. For a scattering volume with a small L , the evanescent mode may "leak" out of the volume. However when we calculate the GPDOS from the scattering matrix, these "leaked" evanescent modes are not explicitly included, leading to a finite ΔN . As we increase L , the evanescent modes decay away, and

is reduced. In a specific example which can be solved exactly [13], a similar form to Eq.(12) was derived which was needed to correct the GPDOS in order to satisfy the precise current conservation. Our numerical study presented here reinforces the results of Ref. [13].

To further investigate the finite size effect to GPDOS, in Fig. (6a,b) we plot the total DOS as obtained by GPDOS and LPDOS as functions of energy, for three system sizes L . The current conservation condition is satisfied very well for most of the first subband energies. When approaching the end of first subband, the current conservation condition is violated gradually, i.e. $\neq 0$. We see that for the smallest scattering region $L = 0$, the agreement of the two total DOS is at best reasonable when the incident electron is from probe I and is away from the second subband edge (Fig. (6a)), and is quite bad when the electron is coming from probe III (Fig. (6b)). The situation improves considerably when we increased the system size. As shown in Fig. (6), for $L = 1$ and $L = 2$, the agreement of the two total DOS are much better. However there is always a divergent behavior near the second subband for all sizes examined if the energy is made very close enough to E_2 . Hence the effect of increasing the size of the scattering volume is to decrease the "critical region" where the two total DOS disagrees.

4 Summary

In conclusion, the low frequency quantum transport properties of a three-probe mesoscopic conductor are studied using Buttiker's current conservation formalism. The static transmission coefficients and emittance matrix of the system with different electric potentials are computed. We found that the behavior of the emittance matrix is closely related to that of the transmission coefficients. We examined the finite size effect of the GPDOS which affects the electric current conservation. In general as the incoming electron energy E approaching the threshold of the second subband, the finite-size GPDOS diverges and the current conservation is violated. The effect of increasing the size of the scattering volume is to decrease the region where the current conservation is violated.

Acknowledgments

We gratefully acknowledge support by a RGC grant from the Government of Hong Kong under grant number HKU 261/95P, a research grant from the Croucher

Foundation, the Natural Sciences and Engineering Research Council of Canada and le Fonds pour la Formation de Chercheurs et l'Aide à la Recherche de la Province du Québec. We thank the Computer Center of the University of Hong Kong for computational facilities and the access of SP2 supercomputer.

References

- [1] See, for example, articles in *Nanostructure Physics and Fabrication*, eds. Mark A. Reed and Wiley P. Kirk, (Academic Press, New York, 1989); F. A. Buot, *Phys. Rep.* 234, 73-174 (1993).
- [2] R. Landauer, *IBM J. Res. Dev.* 1, 223 (1957).
- [3] M. Buttiker, *Phys. Rev. B* 38, 9375 (1988); *Phys. Rev. Lett.* 57, 1761 (1986).
- [4] See, for instance, N. S. Wingreen, A. Jauho and Meir, *Phys. Rev. B* 48, 8487 (1993); T. K. Ng, *Phys. Rev. Lett.* 76, 487 (1996); T. Ivanov, *J. Phys. Condens. Matter* 8, 3427 (1996).
- [5] H. U. Baranger and A. D. Stone, *Phys. Rev. B* 40, 8169 (1989); D. S. Fisher and P. A. Lee, *Phys. Rev. B* 23, 6851 (1981); J. Cohen and Y. Avishai, *J. Phys. Condens. Matter* 7, L121 (1995).
- [6] M. Buttiker, A. Prêtre and H. Thomas, *Phys. Rev. Lett.* 70, 4114 (1993); M. Buttiker and H. Thomas, in *Quantum-Electro Physics, Electronics and Applications*, Eds. K. Ismail et. al., (Institute of Physics Conference Series Number 127, Bristol, 1992), pp. 19.
- [7] M. Buttiker, H. Thomas and A. Prêtre, *Z. Phys. B* 94, 133 (1994).
- [8] T. Christen and M. Buttiker, *Phys. Rev. B* 53, 2064 (1996); and preprint.
- [9] M. Buttiker, *J. Phys. Condens. Matter* 5, 9361 (1993).
- [10] T. Christen and M. Buttiker, *Phys. Rev. Lett.* 77, 143 (1996).
- [11] M. Buttiker and T. Christen, cond-mat/9607051.
- [12] Jian Wang and Hong Guo, *Phys. Rev. B* 54, R11090 (1996).
- [13] Jian Wang, Qingrong Zheng, and Hong Guo, to appear in *Phys. Rev. B*. (April 15 issue, 1997).

- [14] Jian Wang, Qingrong Zheng, and Hong Guo, cond-mat/9610180, to appear in Phys. Rev. B.
- [15] H. Q. Wei, N. J. Zhu, Jian Wang and Hong Guo, submitted to Phys. Rev. B. (1996).
- [16] C. C. Wan, J.-L. Mozos, G. Taraschi, Jian Wang, and Hong Guo, submitted to Phys. Rev. Lett. (1997).
- [17] M. Buttiker, Phys. Rev. B 23, 1846 (1985); 33, 3020 (1986).
- [18] V. Gasparian, T. Christen and M. Buttiker, Phys. Rev. A 54, 4022 (1996).
- [19] M. Buttiker and T. Christen, in Quantum Transport in Semiconductor Submicron Structures, p263, Ed. B Kramer, (Kluwer Academic Pub., Netherlands, 1996); "Dynamic and nonlinear transport in mesoscopic structures", to appear in Theory of Transport Properties of Semiconductor Nanostructures, ed. E. Scholl (Chapman and Hall, London, 1996).
- [20] Y. Avishai and Y. B. Band, Phys. Rev. B 32, 2674 (1985).
- [21] M. Buttiker, Phys. Rev. B 27, 6178 (1983).
- [22] Jian Wang, Yongjiang Wang, and Hong Guo, Appl. Phys. Lett. 65, 1793 (1994).
- [23] G. Iannaccone, Phys. Rev. B 51 4727 (1995).
- [24] V. Gasparian, M. Ortuño, J. Ruiz, E. Cuevas, M. Pollak, Phys. Rev. B 51, 6743 (1995).

Figure Captions

- Figure 1. Schematic plot of the 3-probe quantum wire system. The scattering volume is defined by the dotted lines.
- Figure 2. The transmission coefficients and the emittance E as functions of the incoming electron energy without the tunneling barriers. (a). Solid line: reflection coefficient R_{11} ; dotted line: transmission coefficient T_{21} ; dashed line: T_{31} . (b). Emittance E . Solid line: E_{11} ; dotted line: E_{21} ; dashed line: E_{31} .
- Figure 3. Electron dwell time τ_1 as a function of the incoming electron energy in the tunneling regime. The three peaks indicate three resonance states in the system in this energy range. Inset: τ_3 .
- Figure 4. The transmission coefficients and the emittance E as functions of the incoming electron energy in the tunneling regime. (a). Solid line: R_{11} ; dotted line: E_{11} ; (b). Solid line: T_{21} ; dotted line: E_{21} ; (c). Solid line: T_{31} ; dotted line: E_{31} .
- Figure 5. (a). The difference, δ_1 , of the total PDOS as computed from the GPDOS and LPDOS from Eq. (11) as a function of the scattering volume linear size L . Solid line: at energy $E = 39.46699$; dotted line: at energy $E = 39.45371$; dashed line: at energy $E = 39.44137$; (b). The quantity, $\ln[\tau_1 = (2L + 1)\hbar k_2]$ as a function of the linear size L for several incoming electron energies as shown. At large L , this quantity approaches unity, confirming the form of Eq. (12).
- Figure 6. Comparison of the total PDOS computed from the GPDOS and LPDOS, as a function of the incoming electron energy for three different sizes $L = 0; 1$, and 2 in the transmissive regime. (a). Electrons coming from probe 1. (b). Electrons coming from probe 3. The agreement of the total PDOS is quite good up to the "critical region" near the onset of the second subband.

Fig.(2a)

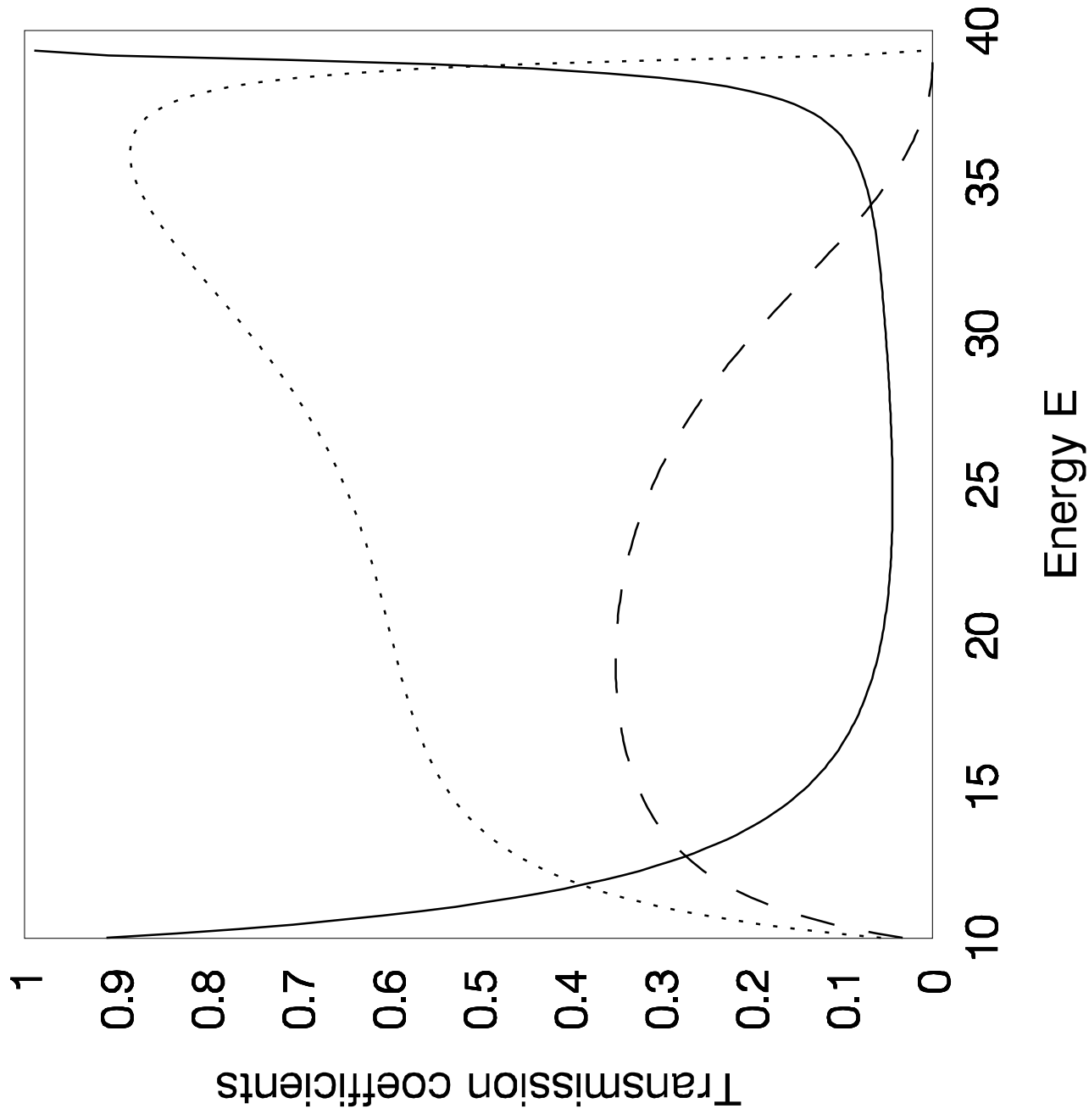
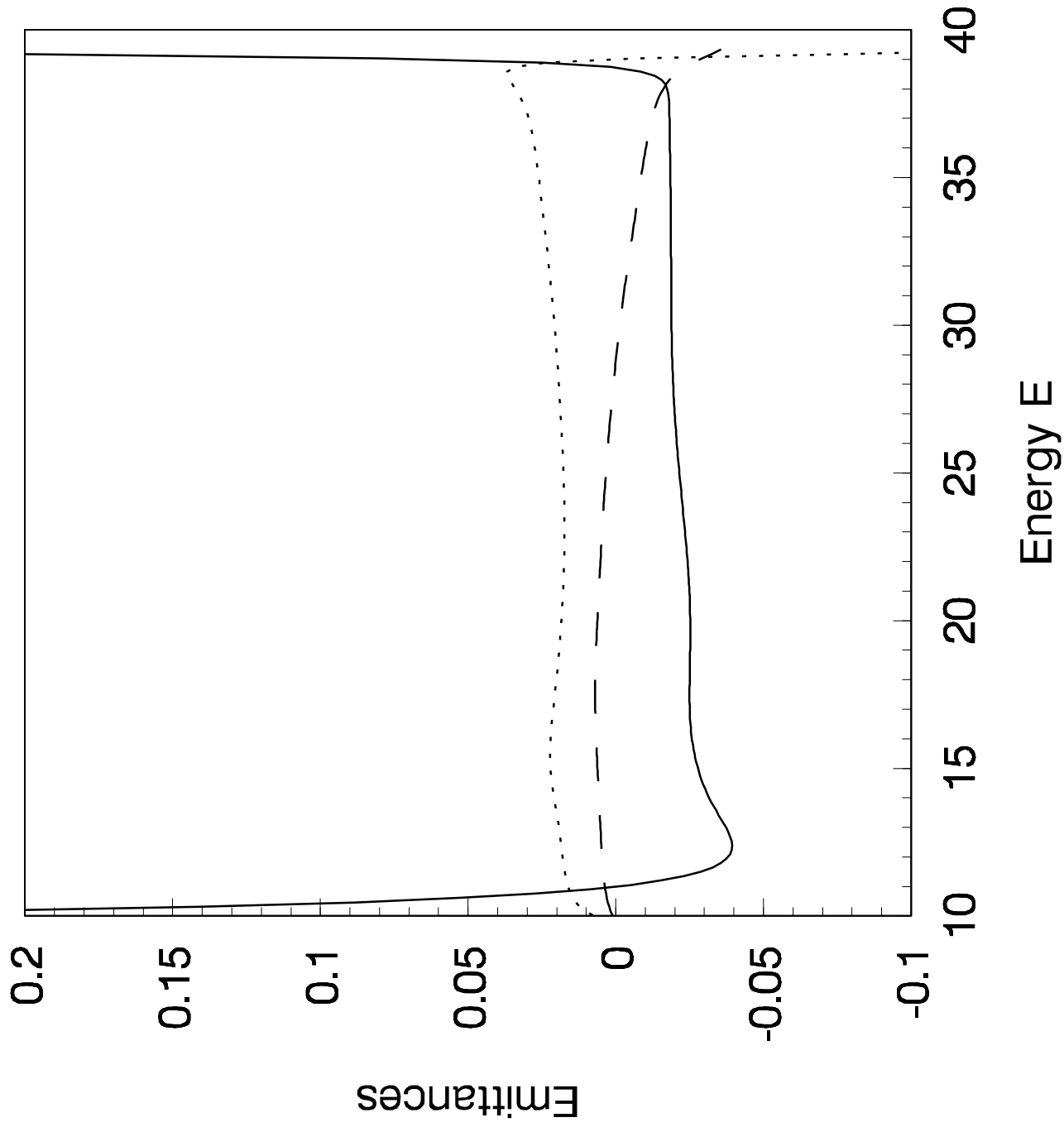
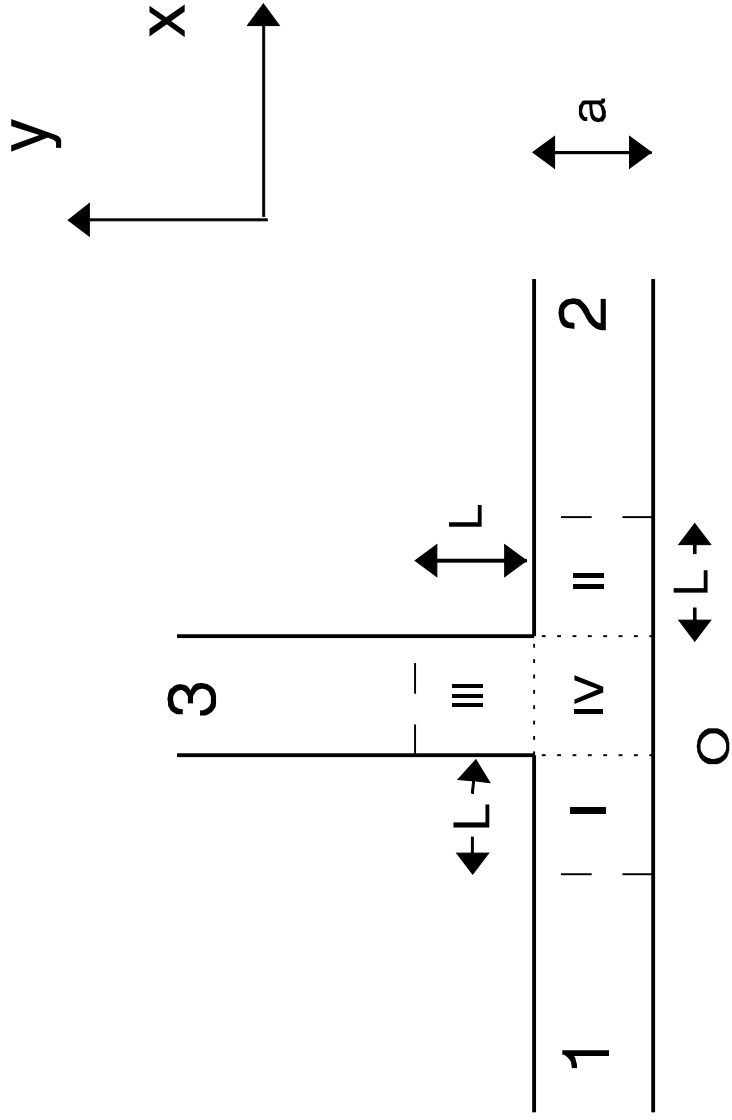


Fig.(2b)





Figure(1)

Fig.(3)

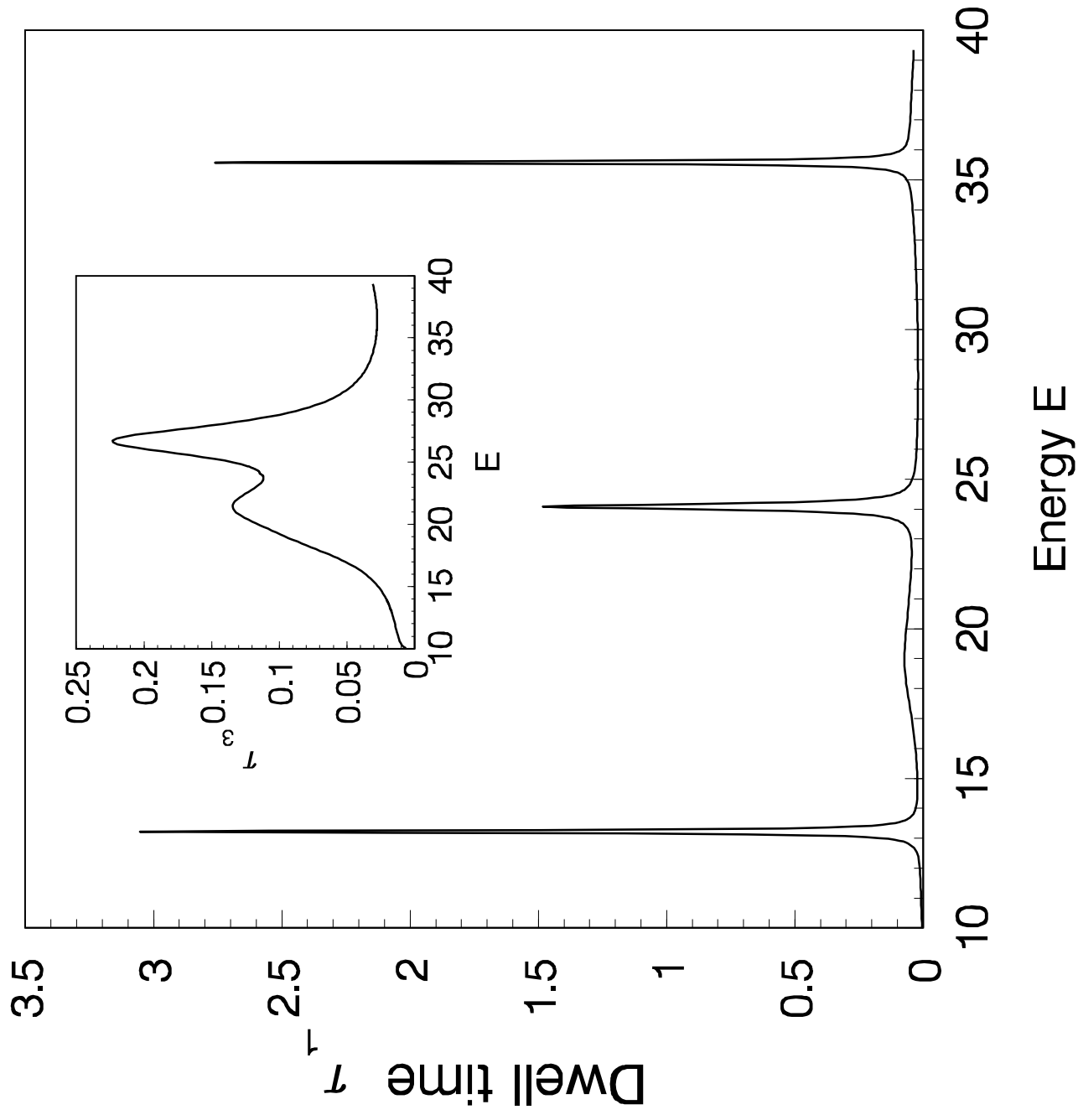


Fig.(4a)

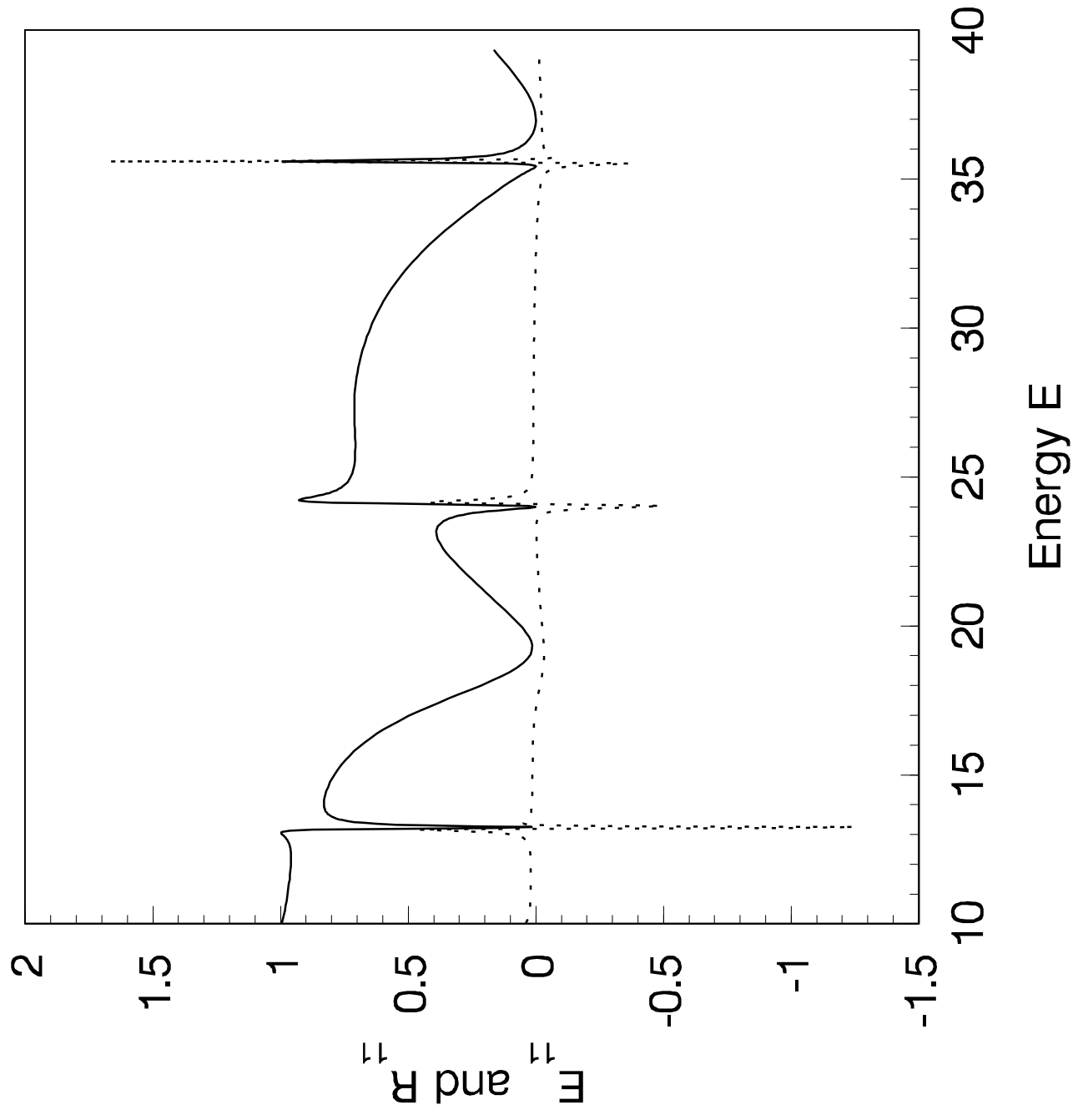


Fig.(4b)

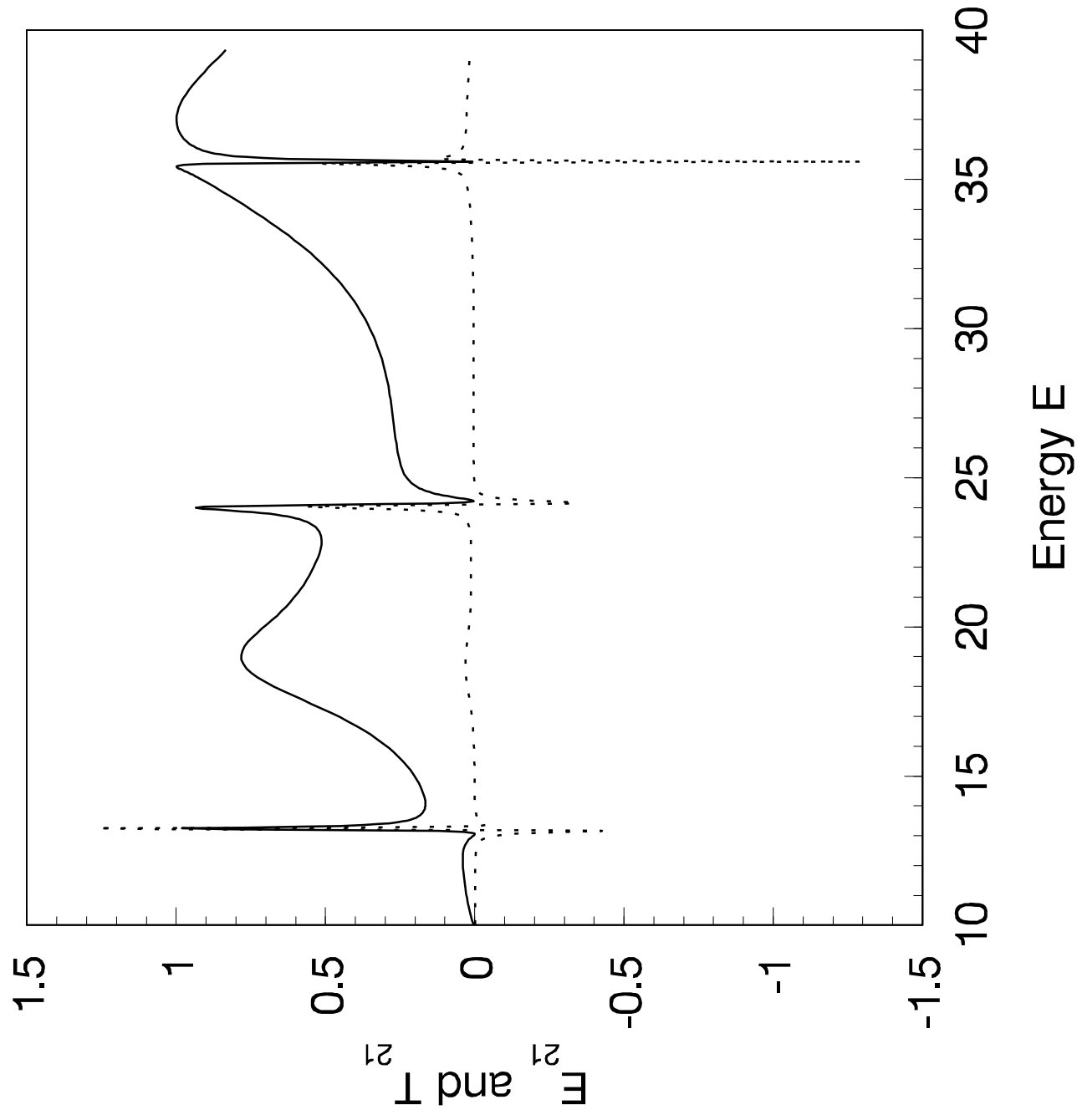


Fig.(4c)

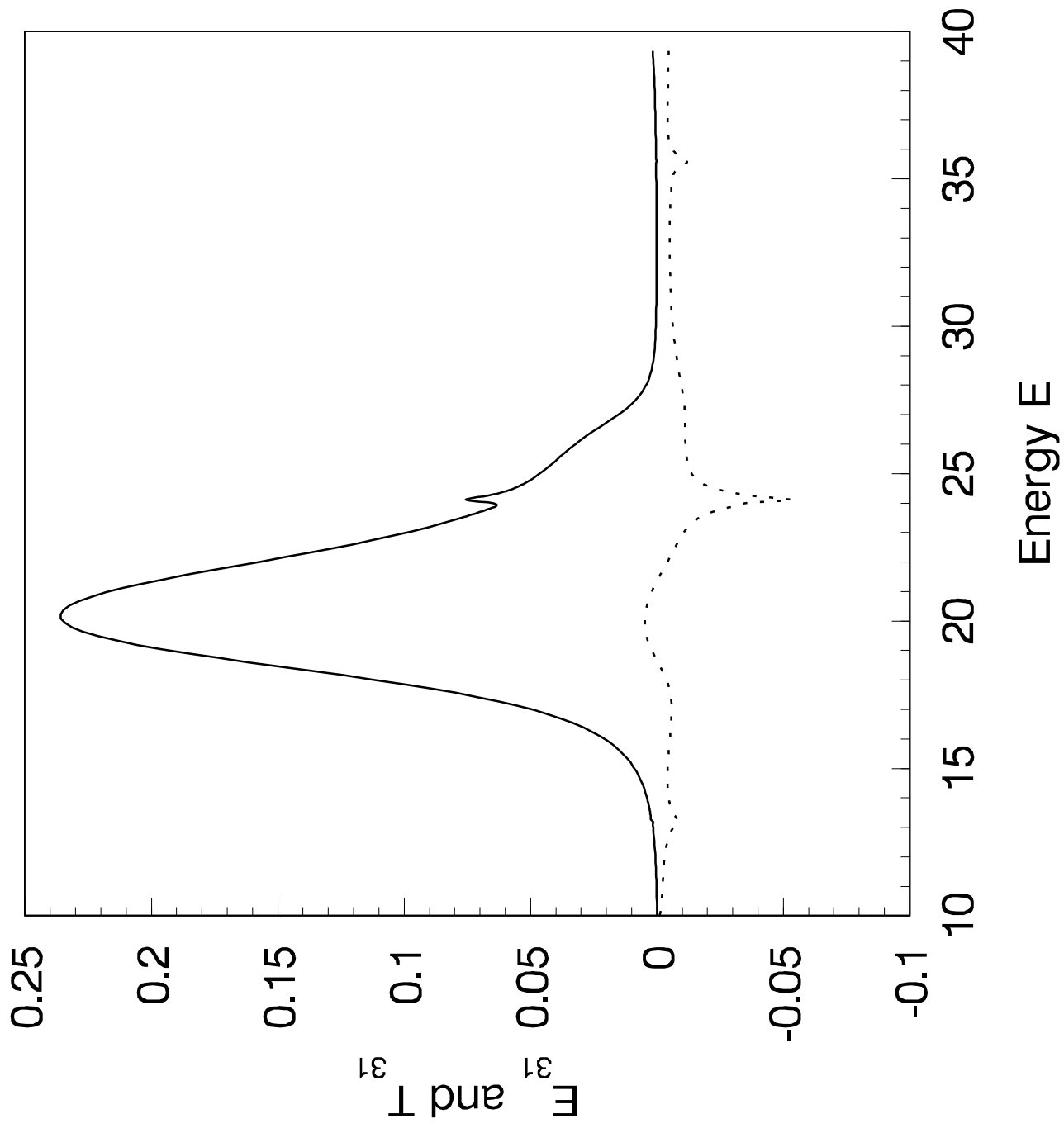


figure (5a)

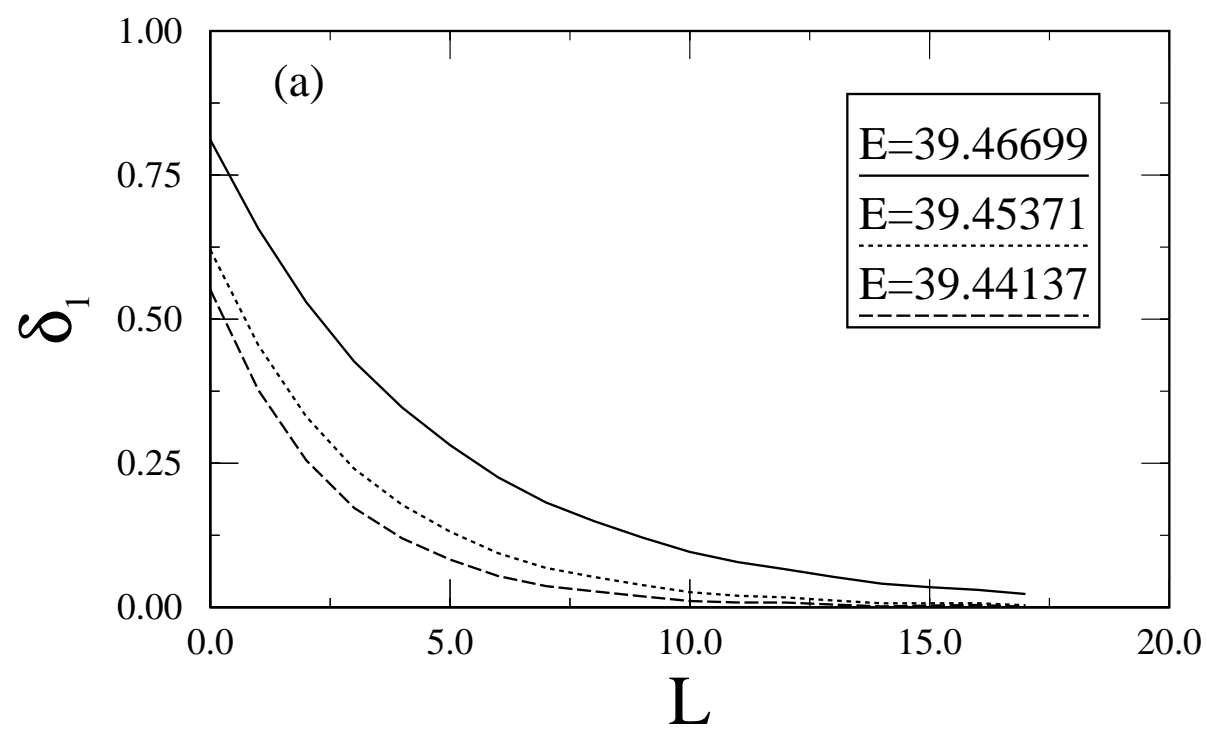


figure (5b)

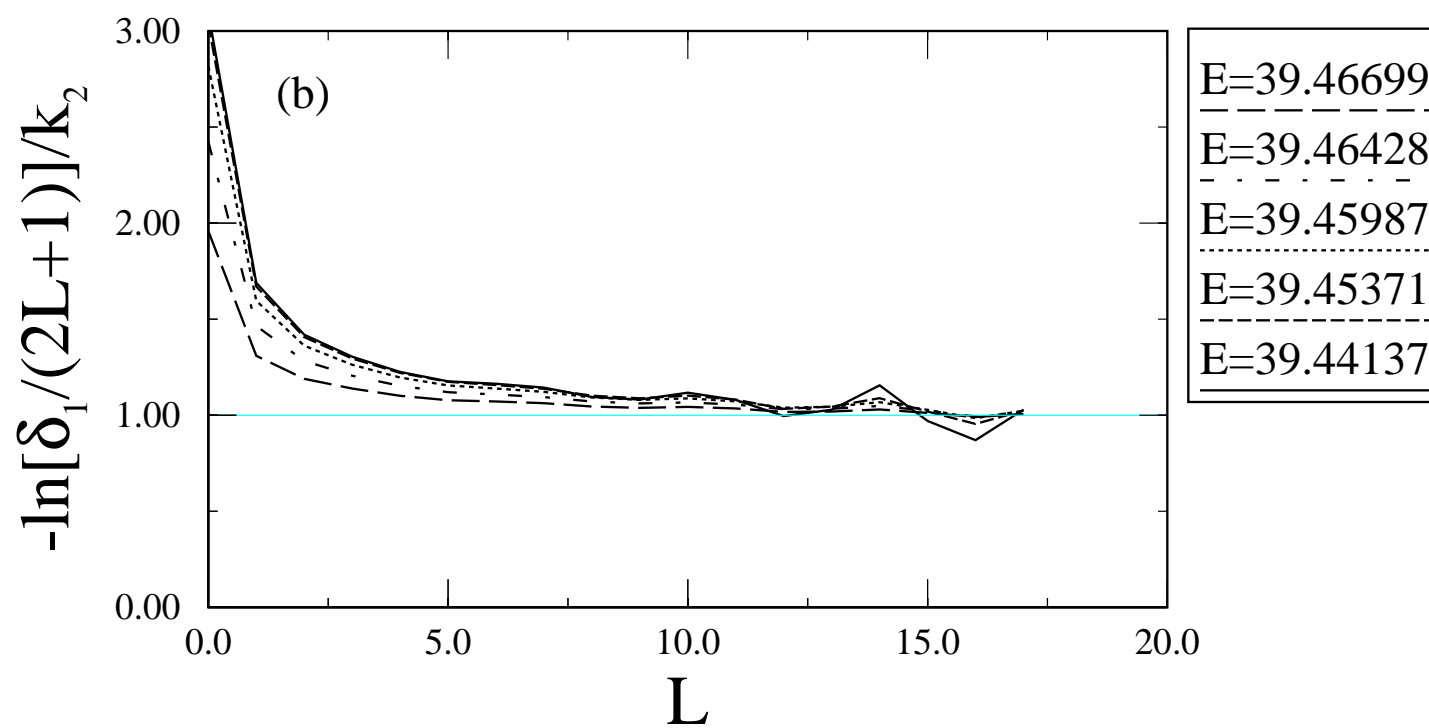


Fig.(6a)

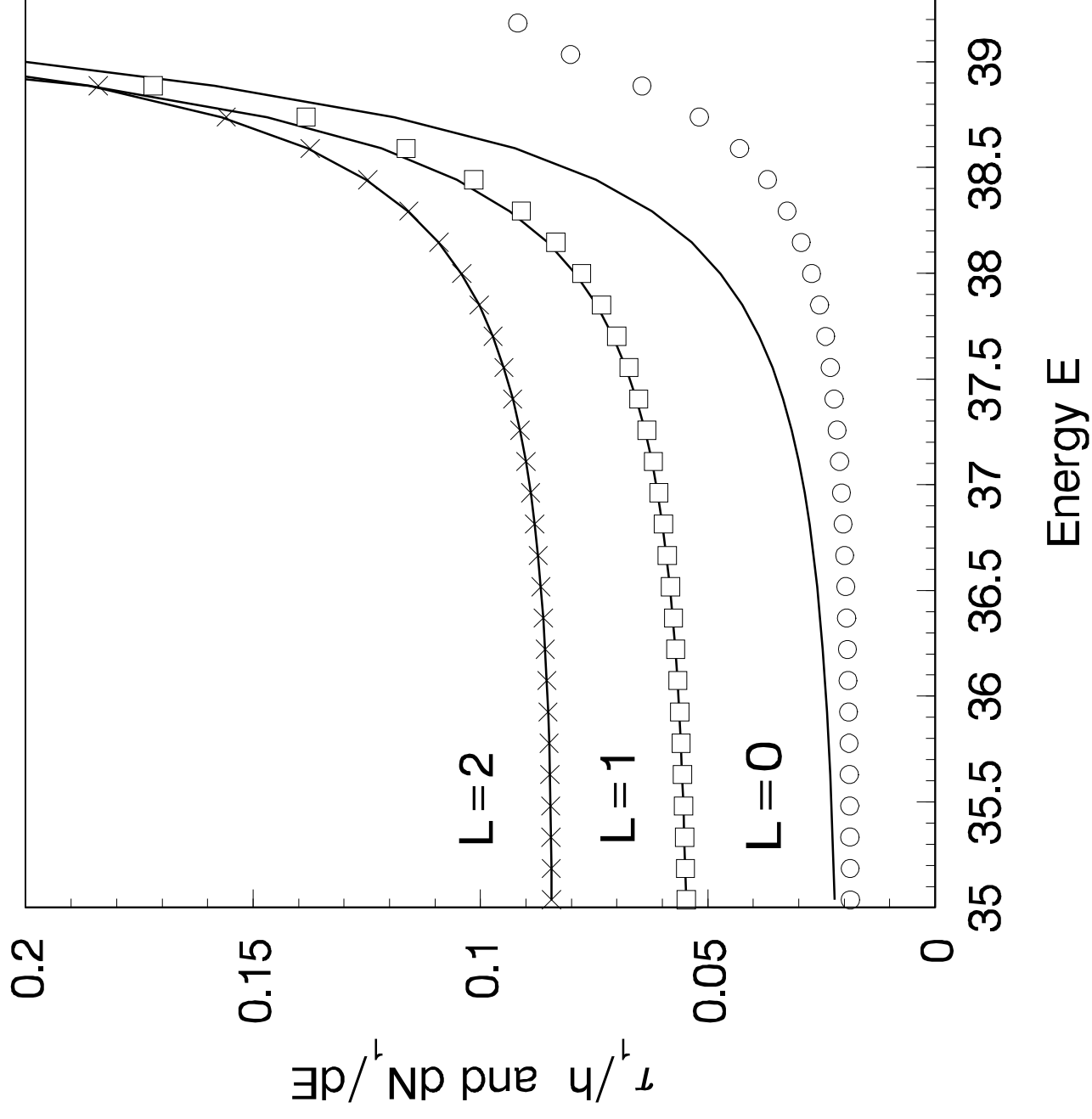


Fig.(6b)

